A Dynamic-Thermodynamic Sea Ice Model on an Arakawa C-Grid for Coupled Ocean/Sea Ice Estimation. Part 1: Sensitivities to formulation of rheology.

Martin Losch [a,1], Dimitris Menemenlis [b], Jean-Michel Campin [c], Patick Heimbach [c], and Chris Hill [c]

[a] *Alfred-Wegener-Institut für Polar- und Meeresforschung, Postfach 120161, 27515 Bremerhaven, Germany*
[b] *Jet Propulsion Laboratory, Pasadena, California, USA*
[c] *Massachusett Institute of Technology, 77 Massachusetts Avenue, Cambridge 02139, USA*

Abstract

As part of an ongoing effort to obtain a best possible, time-evolving analysis of most available ocean and sea ice data, a dynamic and thermodynamic sea-ice model has been coupled to the Massachusetts Institute of Technology general circulation model (MITgcm). Ice mechanics follow a viscous-plastic rheology and the ice momentum equations are solved numerically using either line-successive-over-relaxation (LSOR) or elastic-viscous-plastic (EVP) dynamic models. Ice thermodynamics are represented using either a zero-heat-capacity formulation or a two-layer formulation that conserves enthalpy. The model includes prognostic variables for snow and for sea-ice salinity. The above sea ice model components were borrowed from current-generation climate models but they were reformulated on an Arakawa C grid in order to match the MITgcm oceanic grid and they were modified in many ways to permit efficient and accurate automatic differentiation. This paper describes the MITgcm sea-ice model; it presents example Arctic and Antarctic results from a realistic, eddy-permitting, global ocean and sea-ice configuration; and it compares B-grid and C-grid dynamic solvers in a regional Arctic configuration.

Key words: NUMERICAL SEA-ICE MODELING, . . .

1. Introduction

It is widely recognized that high-latitude processes are an important component of the climate system (Lemke et al., 2007). As a consequence, these processes need to be accurately represented in present-day global climate state estimates and in prediction models. One of the main drivers of high-latitude processes is sea-ice. Its variability and long term trends are distinctly different in the polar regions of the Northern and the Southern hemispheres (Cavalieri and Parkinson, 2008, Parkinson and Cavalieri, 2008). These differences and their interaction with the global climate system are still poorly understood and call for a dynamical explanation (**?**). Both the atmospheric and oceanic states to which the sea-ice is coupled are still largely uncertain, yet driving a sea-ice model requires both to be known accurately. Sea-ice in turn constrains the state of both ocean and atmosphere near the surface so that sea-ice observations contain valuable information about the state of the coupled system. Therefore, its is a natural objective to build an estimation system with a coupled ocean/sea-ice model that is capable of using both sea-ice and ocean observations to obtain a dy-

[1] corresponding author, email: Martin.Losch@awi.de, ph: ++49 (471) 4831-1872, fax: ++49 (471) 4831-1797

namically consistent ocean/sea-ice state with closed property budgets that can be analyzed in terms of its inter-annual to decadal variations.

For the ocean without sea-ice, such an estimation system has been created by the *Circulation and Climate of the Ocean* (ECCO) consortia. Estimates of the time-evolving ocean circulation, constrained by a multitude of in-situ and remotely sensed global observations, are now routinely available and are being applied to myriad scientific problems (Wunsch and Heimbach, 2007, Heimbach and Wunsch, 2007, and references therein). At the heart of this approach is the formulation of a least-squares optimization problem to fit the Massachusetts Institute of Technology general circulation model (MITgcm) to as many observations as practical using either Kalman filter/RTS smoother (Fukumori, 2002), Green's functions (Menemenlis et al., 2005a), or adjoint methods. Of particular interest here is the adjoint or Lagrange multiplier method. This method allows the efficient calculation of gradients in a very high-dimensional space to be used in gradient-based solution techniques of least-squares minimization problems. It has also been recognized that the adjoint model by itself provides a very powerful research tool to conduct dynamical sensitivity analyses (e.g., Marotzke et al., 1999, Dutkiewicz et al., 2006, Losch and Heimbach, 2007, **?**).

This paper describes a new sea-ice model designed to be used for coupled sea-ice/ocean state estimation. The lack *[can we delete this?: , until recently,]* of an interactive sea-ice component in the ECCO approach, the experience gained with the ocean-only problem and its success, the necessity of representing polar and sub-polar interactions in ECCO-type calculations, the need to incorporate sea-ice observations into the estimation system, and the requirement to generate efficient adjoint code, collectively make a compelling case for the development of a such new sea-ice model. While many of its features are "conventional" (yet for the most part state-of-the-art), the model is different from previous models in that it is tailored for the generation of efficient adjoint code for coupled ocean/sea-ice simulations by means of automatic (or algorithmic) differentiation (AD, Griewank, 2000). Sensitivity propagation in coupled systems is highly desirable as it permits both sea-ice and ocean observations to be used as simultaneous constraints yielding a truly coupled estimation problem. Mainly for this reason, the sea-ice model architecture is tightly coupled to that of the MITgcm for which there is extensive experience with automatic adjoint code generation.

The present work is a first step towards adding sea-ice capability to the ECCO estimates. Following the experience gained with the MITgcm, namely (1) the development and description of a reliable forward model (in the case of the MITgcm the works of Marshall et al., 1997a,b), as well as (2) demonstration that reliable and interpretable sensitivities can be computed via its adjoint (for MITgcm the work of Marotzke et al., 1999), the paper consists of two parts: Part 1 (this paper) outlines the development of a dynamic and thermodynamic sea ice model that has been coupled to the MITgcm, with special emphasis on the implementation of the sea-ice rheology solvers, and description of its behavior for various parameter options. The forward model borrows many components from current-generation sea-ice models. Although these components are modified in many ways to permit efficient and accurate automatic differentiation, the results of sensitivity studies with this model are general and can be carried over to other sea-ice models. Part 2 (a companion paper) is devoted to the development of an efficient coupled ocean/sea-ice adjoint by means of automatic differentiation and to the demonstration of its use in sensitivity calculations related to the parameter choices in Part 1.

Most standard sea-ice models are discretized on Arakawa-B grids (e.g., Hibler, 1979, Harder and Fischer, 1999, Kreyscher et al., 2000, Zhang et al., 1998, Hunke and Dukowicz, 1997), probably because early numerical ocean models were formulated on the Arakawa-B grid and because of the easier (implicit) treatment of the Coriolis term. As model resolution increases, more and more ocean and sea ice models use an Arakawa-C grid discretization (e.g., Marshall et al., 1997a, Ip et al., 1991, Tremblay and Mysak, 1997, Lemieux et al., 2008). The new MIT sea-ice model is formulated on an Arakawa C-grid, and two different solvers are implemented; a previous verion on a B-grid is also available. Hence, the model suggests itself to comparing different grids and solvers within the same numerical architecture.

From the perspective of coupling a sea ice-model to a C-grid ocean model, the exchange of fluxes of heat and fresh-water pose no difficulty for a B-grid sea-ice model (e.g., Timmermann et al., 2002). However, surface stress is defined at velocity points and thus needs to be interpolated between a B-grid sea-ice model and a C-grid ocean model. Smoothing implicitly associated with this interpolation may mask grid scale noise and may contribute to stabilizing the solution. On the other hand, the stress signals are damped by smoothing which may lead to reduced variability of the system. By choosing a C-grid for the sea-ice model, we avoid this difficulty altogether and render the stress coupling as consistent as the buoyancy flux coupling.

A further characteristic of the C-grid formulation is apparent in narrow straits. In the limit of only one grid cell between coasts there is no flux allowed for a B-grid (with no-slip lateral boundary counditions, which are natural for the B-grid), and models have used topographies with artificially widened straits to avoid this problem (Holloway et al., 2007). The C-grid formulation on the other hand allows a flux of sea-ice through narrow passages even if no-slip boundary conditions are imposed. We demonstrate this effect in the Canadian Arctic Archipelago (CAA).

The present Part 1 explores differences between the solutions obtained on either grid, with either solver, and under various options for lateral boundary conditions (free-slip vs. no-slip). Such types of model sensitivities are configuration-based, rather than exploring a continuous parameter space, and are best assessed in separate forward calculations.

One crucial element of the adjoint is the notion of *tangent* linearity in case of an exact adjoint as derived and used here, that is, the adjoint state depends on the exact time-varying model state around which it is linearized. Adjoint calculations are thus tightly linked to the forward model configuration, and sensitivity calculations for different calculations need to be compared. The calculations presented here provide crucial baseline scenarios for Part 2.

The remainder of Part 1 focusses on the forward model and its configuration sensitivities with regard to the treatment of sea-ice rheology. Section 2 describes the MITgcm sea ice model (MITsim) in more detail. Example results are presented for the Arctic, taken from a realistic, eddy-permitting, global ocean and sea-ice configuration (Section 3). We compare B-grid and C-grid dynamical solvers under different lateral boundary conditions and investigate further aspects of sea-ice modeling in a regional Arctic configuration. Conclusion and recommedations are presented in Section 4.

2. Model Formulation

The MITgcm sea ice model (MITsim) is based on a variant of the viscous-plastic (VP) dynamic-thermodynamic sea-ice model of Zhang and Hibler (1997) first introduced by Hibler (1979, 1980). In order to adapt this model to the requirements of coupled ice-ocean simulations, many important aspects of the original code have been modified and improved:

– the code has been rewritten for an Arakawa C-grid, both B- and C-grid variants are available; the C-grid code allows for no-slip and free-slip lateral boundary conditions;
– two different solution methods for solving the nonlinear momentum equations have been adopted: LSOR (Zhang and Hibler, 1997), EVP (Hunke and Dukowicz, 1997, Hunke, 2001);
– ice-ocean stress can be formulated as in Hibler and Bryan (1987);
– ice variables can be advected by sophisticated, conservative advection schemes with flux limiters;
– growth and melt parameterizations have been refined and extended in order to allow for automatic differentiation of the code.

The sea ice model is tightly coupled to the ocean compontent of the MITgcm (Marshall et al., 1997a, MITgcm Group, 2002). Heat, fresh water fluxes and surface stresses are computed from the atmospheric state and modified by the ice model at every time step. The remainder of this section describes the model equations and details of their numerical realization. Further documentation and model code can be found at `http://mitgcm.org`.

2.1. *Dynamics*

Sea-ice motion is driven by ice-atmosphere, ice-ocean and internal stresses. The internal stresses are evaluated following a viscous-plastic (VP) constitutive law with an elliptic yield curve as in Hibler (1979). The full momentum equations for the sea-ice model and the solution by line successive over-relaxation (LSOR) are described in Zhang and Hibler (1997). Alternatively, the momentum equation can be solved with an elastic-viscous-plastic (EVP) solver following Hunke (2001). In this technique, evolution equations for the internal stress tensor components are solved by sub-cycling within one time step.

In both cases, the bulk viscosities can be bounded from above (if required for numerical reasons). For stress tensor computations the replacement pressure (Hibler and Ip, 1995) is used so that the stress state always lies on the elliptic yield curve by definition. Alternatively, in the so-called truncated ellipse method (TEM) the shear viscosity is capped to suppress any tensile stress (Hibler and Schulson, 1997, Geiger et al., 1998).

The horizontal gradient of the ocean's surface is estimated directly from ocean sea surface height and pressure loading from atmosphere, ice and snow (Campin et al., 2008); ice does not float on top of the ocean, but within the ocean according to its buoyancy.

Lateral boundary conditions are naturally "no-slip" for B-grids, as the tangential velocities points lie on the boundary. For C-grids, the lateral boundary condition for tangential velocities is realized via "ghost points", allowing alternatively no-slip or free-slip conditions. In ocean models free-slip boundary conditions in conjunction with piecewise-constant ("castellated") coastlines have been shown to reduce to no-slip boundary conditions (Adcroft and Marshall, 1998); for sea-ice models the effects of lateral boundary conditions have not yet been studied (as far as we know).

Moving sea ice exerts a surface stress on the ocean. In coupling the sea-ice model to the ocean model, this stess is applied directly to the surface layer of the ocean model. An alternative ocean stress formulation is given by Hibler and Bryan (1987). Rather than applying the interfacial stress directly, the stress is derived from integrating over the ice thickness to the bottom of the oceanic surface layer. In the resulting equation for the *combined* ocean-ice momentum, the interfacial stress cancels and the total stress appears as the sum of windstress and divergence of internal ice stresses (see also Eq. 2 of Hibler and Bryan, 1987). While this formulation tightly embeds the sea-ice into the surface layer of the ocean, its disadvantage is that now the velocity in the surface layer of the ocean that is used to advect ocean tracers, is really an average over the ocean surface velocity and the ice velocity leading to an inconsistency as the ice temperature and salinity are different from the oceanic variables. Both stress coupling options are available for a direct comparison of the their effects on the sea-ice solution.

The discretization of the momentum equestion is straightforward. It is similar to that of Zhang et al. (1998), Zhang and Rothrock (2003), but differs fundamentally in the underlying grid, namely the Arakawa C-grid. The EVP model, in particular, is discretized naturally on the C-grid with the diagonal components of the stress tensor on the center points and the off-diagonal term on the corner (or vorticity) points of the grid. With this choice all derivatives are discretized as central differences and very little averaging is involved. Apart from the standard C-grid implementation, the original B-grid implementation of Zhang and Hibler (1997) is also available as an option in the code.

2.2. *Thermodynamics*

In its original formulation the sea ice model (Menemenlis et al., 2005b) uses simple thermodynamics following the appendix of Semtner (1976). This formulation does not allow storage of heat, that is, the heat capacity of ice is zero. Upward conductive heat flux is parameterized assuming a linear temperature profile and a constant ice conductivity. This type of model is often refered to as a "zero-layer" model. The surface heat flux is computed in a similar way to that of Parkinson and Washington (1979) and Manabe et al. (1979).

The conductive heat flux depends strongly on the ice thickness h. However, the ice thickness in the model represents a mean over a potentially very heterogeneous thickness distribution. In order to parameterize a sub-grid scale distribution for heat flux computations, the mean ice thickness h is split into seven thickness categories H_n that are equally distributed between $2h$ and a minimum imposed ice thickness of 5 cm by $H_n = \frac{2n-1}{7}\,h$ for $n \in [1,7]$. The heat fluxes computed for each thickness category is area-averaged to give the total heat flux (Hibler, 1984).

The atmospheric heat flux is balanced by an oceanic heat flux from below. The oceanic flux is proportional to the difference between ocean surface temperature and the freezing point temperature of sea water, which is a function of salinity. Contrary to Menemenlis et al. (2005b), this flux is not assumed to instantaneously melt or create ice, but a time scale of three days is used to relax the ocean temperature to the freezing point (**?**). While this parameterization is not new (it follows the ideas of e.g., Mellor et al., 1986, McPhee, 1992, Lohmann and Gerdes, 1998, Notz et al., 2003), it avoids a discontinuity in the functional relationship between model variables, which is cruical for making the code differentiable for adjoint code generation (**?**). The parameterization of lateral and vertical growth of sea ice follows that of Hibler (1979, 1980).

On top of the ice there is a layer of snow that modifies the heat flux and the albedo as in Zhang et al. (1998). If enough snow accumulates so that its weight submerges the ice and the snow is flooded, a simple mass conserving parameterization of snow-ice formation (a flood-freeze algorithm following Archimedes' principle) turns snow into ice until the ice surface is back at $z = 0$ (Leppäranta, 1983).

The concentration c, effective ice thickness (ice volume per unit area, $c \cdot h$), and effective snow thickness ($c \cdot h_s$) are advected by ice velocities. From the various advection scheme that are available in the MITgcm (MITgcm Group, 2002), we choose flux-limited schemes (multidimensional 2nd and 3rd-order advection scheme with flux limiter, Roe, 1985, Hundsdorfer and Trompert, 1994) to preserve sharp gradients and edges that are typical of sea ice distributions and to rule out unphysical over- and undershoots (negative thickness or concentration). These scheme conserve volume and horizontal area and are unconditionally stable, so that no extra diffusion is required. The original 2nd order central differences scheme requires additional diffusion and is used here for comparison.

Finally, there is considerable doubt about the reliability of a "zero-layer" thermodynamic model—Semtner (1984) found significant errors in phase (one month lead) and amplitude (≈50% overestimate) in such models—, so that today many sea ice models employ more complex thermodynamics. A popular thermodynamics model of Winton (2000) is implemented in the MITsim. It is based on the 3-layer model of Semtner (1976) and treats brine content by means of enthalphy conservation. This model requires additional state variables, namely the enthalphy of the two ice layers, to be advected by ice velocities. *[Jean-Michel, your turf:]Care must be taken in advecting these quantities in order to ensure conservation of enthalphy. Currently this can only be accomplished with a 2nd-order advection scheme with flux limiter (Roe, 1985).*

3. Forward Sensitivity Experiments in an Arctic Domain with Open Boundaries

This section presents results from regional coupled ocean and sea ice simulations of the Arctic Ocean that exercise various capabilities of the MITgcm sea ice model. The objective is to compare the old B-grid LSOR dynamic solver with the new C-grid LSOR and EVP solvers. Additional experiments are carried out to illustrate the differences between different ice advection schemes, ocean-ice stress formulations and the two main options for sea ice thermodynamics in the MITgcm.

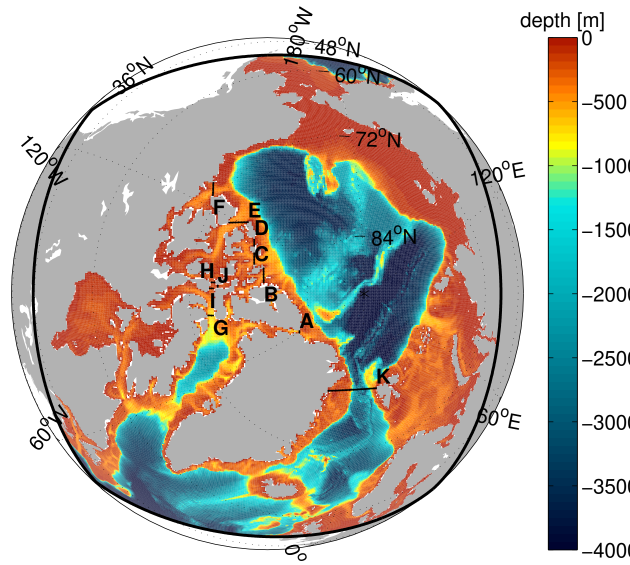

Fig. 1. Left: Bathymetry and domain boundaries of Arctic Domain. The letters in the inset label sections in the Canadian Archipelago, where ice transport is evaluated: A: Nares Strait; B: *Meighen Island*; C: Prince Gustaf Adolf Sea; D: *Brock Island*; E: M'Clure Strait; F: Amundsen Gulf; G: Lancaster Sound; H: Barrow Strait *W.*; I: Barrow Strait *E.*; J: Barrow Strait *N.*; K: Fram Strait. The sections A through F comprise the total inflow into the Canadian Archipelago. *[May still need to check the geography.]*

3.1. *Model configuration and experiments*

The Arctic model domain is illustrated in Figure 1. It has 420 by 384 grid boxes and is carved out, and obtains open boundary conditions from, a global cubed-sphere configuration similar to that described in Menemenlis et al. (2005b).

*[Some of this could be part of the introduction?]*The global ocean and sea ice results presented in Menemenlis et al. (2005b) were carried out as part of the Estimating the Circulation and Climate of the Ocean, Phase II (ECCO2) project. ECCO2 aims to produce increasingly accurate syntheses of all available global-scale ocean and sea-ice data at resolutions that start to resolve ocean eddies and other narrow current systems, which transport heat, carbon, and other properties within the ocean (Menemenlis et al., 2005b). The particular ECCO2 simulation from which we obtain the boundary conditions is a baseline 28-year (1979-2006) integration, labeled cube76, which has not yet been con-

strained by oceanic and by sea ice data. A cube-sphere grid projection is employed, which permits relatively even grid spacing throughout the domain and which avoids polar singularities (Adcroft et al., 2004). Each face of the cube comprises 510 by 510 grid cells for a mean horizontal grid spacing of 18 km. There are 50 vertical levels ranging in thickness from 10 m near the surface to approximately 450 m at a maximum model depth of 6150 m. The model employs the partial-cell formulation of Adcroft et al. (1997), which permits accurate representation of the bathymetry. Bathymetry is from the S2004 (W. Smith, unpublished) blend of the Smith and Sandwell (1997) and the General Bathymetric Charts of the Oceans (GEBCO) one arc-minute bathymetric grid. The model is integrated in a volume-conserving configuration using a finite volume discretization with C-grid staggering of the prognostic variables. In the ocean, the non-linear equation of state of Jackett and McDougall (1995) is used. The global ocean model is coupled to a sea ice model in a configuration similar to the case C-LSR-ns (see Table 1), with open water, dry ice, wet ice, dry snow, and wet snow albedos of, respectively, 0.15, 0.88, 0.79, 0.97, and 0.83.

This particular ECCO2 simulation is initialized from temperature and salinity fields derived from the Polar science center Hydrographic Climatology (PHC) 3.0 (Steele et al., 2001). Surface boundary conditions for the period January 1979 to July 2002 are derived from the European Centre for Medium-Range Weather Forecasts (ECMWF) 40 year re-analysis (ERA-40) (Uppala et al., 2005). Surface boundary conditions after September 2002 are derived from the ECMWF operational analysis. There is a one month transition period, August 2002, during which the ERA-40 contribution decreases linearly from 1 to 0 and the ECMWF analysis contribution increases linearly from 0 to 1. Six-hourly surface winds, temperature, humidity, downward short- and long-wave radiations, and precipitation are converted to heat, freshwater, and wind stress fluxes using the Large and Pond (1981, 1982) bulk formulae. Shortwave radiation decays exponentially as per Paulson and Simpson (1977). Low frequency precipitation has been adjusted using the pentad (5-day) data from the Global Precipitation Climatology Project (GPCP, Huffman et al., 2001). The time-mean river run-off from Large and Nurser (2001) is applied globally, except in the Arctic Ocean where monthly mean river runoff based on the Arctic Runoff Data Base (ARDB) and prepared by P. Winsor (personnal communication, 2007) is specificied. Additionally, there is a relaxation to the monthly-mean climatological sea surface salinity values from PHC 3.0, a relaxation time scale of 101 days.

Vertical mixing follows Large et al. (1994) but with meridionally and vertically varying background vertical diffusivity; at the surface, vertical diffusivity is 4.4×10^{-6} m^2 s^{-1} at the Equator, 3.6×10^{-6} m^2 s^{-1} north of 70°N, and 1.9×10^{-5} m^2 s^{-1} south of 30°S and between 30°N and 60°N , with sinusoidally varying values in between these latitudes; vertically, diffusivity increases to 1.1×10^{-4} m^2 s^{-1} at a a depth of 6150 m as per Bryan and Lewis (1979). A 7th-order monotonicity-preserving advection scheme (Daru and Tenaud, 2004) is employed and there is no explicit horizontal diffusivity. Horizontal viscosity follows Leith (1996) but modified to sense the divergent flow (Fox-Kemper and Menemenlis, 2008).

As an example result we show the effective ice thickness distribution in March and September, averaged over the years 1992–2002, in Figure 2. The ice edge estimated as the 15% isoline of SSMI ice concentation observations (obtained from `http://nsidc.org`) is drawn as a gray contour line for comparison. The overall agreement of the position of the ice-egde is good. The model appears to overestimate the ice-extent systematically, but this apparent overestimation is emphasized by the fact that through averaging ice thickness can be non-zero for very small ice concentrations[, AND WE SHOULD PROBABLY MASKS ALL HEFF VALUES FOR MEAN(AREA)¡.15 TO GET RID OF THIS PROBLEM.]

The model configuration of cube76 carries over to the Arctic domain configuration except for numerical details related to the non-linear free surface that are not supported by the open boundary code, and the albedos of open water, dry ice, wet ice, dry snow, and wet snow, which are now, respectively, 0.15, 0.85, 0.76, 0.94, and 0.8.

The model is integrated from Jan 01, 1992 to Mar 31, 2000. Table 1 gives an overview over the experiments discussed in Section 3.2. Both LSOR and EVP solvers solve the same viscous-plastic rheology, so that differences between runs B-LSR-ns, C-LSR-ns, and C-EVP-ns can be interpreted as pure model error. Lateral boundary conditions on a coarse grid (coarse compared to the roughness of the true coast line) are unclear, so that comparing the no-slip solutions to the free-slip solutions gives another measure of uncertainty in sea ice modeling. The remaining experiments explore further sensitivities of the sys-

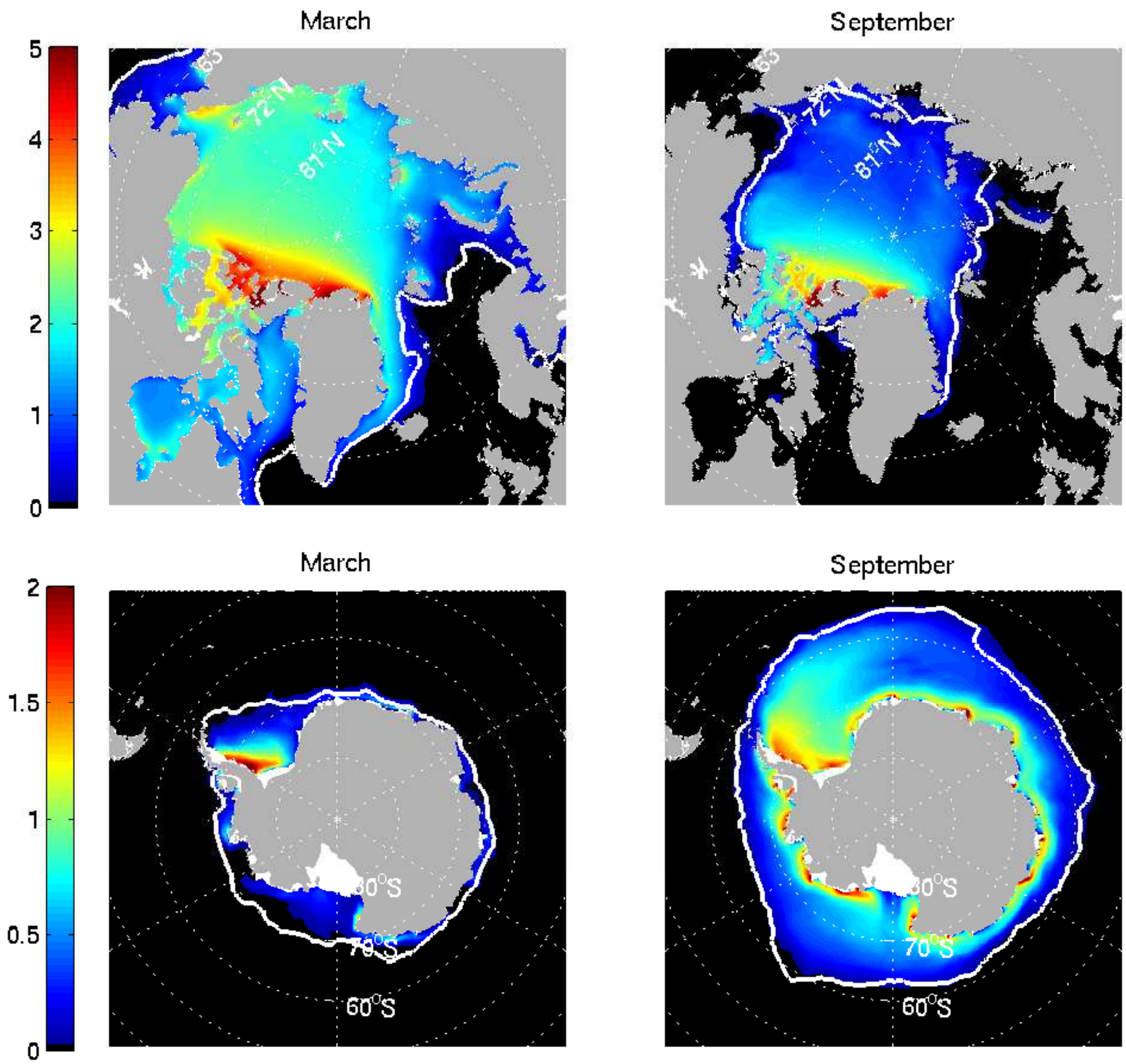

Fig. 2. Global simulation cube76: Effective ice thickness distribution (color) and the 15% isoline of SSMI ice concentation observations (gray contour line), averaged over the years 1992–2002. The top row shows the results for the Arctic Ocean, the bottom row for the Antarctic Oceans; the left column shows distributions for March, the right column for September. Note the different color scales for top and bottom rows.

tem to different physics (change in rheology, advection and diffusion properties, stress coupling, and thermodynamics) and different time steps for the EVP solutions: Hunke (2001) uses 120 subcycling steps for the EVP solution. We use two interpretations of this choice where the EVP model is subcycled 120 times within a (short) model timestep of 1200 s resulting in a very long and expensive integration ($\Delta t_{\mathrm{evp}} = 10\,\mathrm{s}$) and 144 times within the forcing timescale of 6 h ($\Delta t_{\mathrm{evp}} = 150\,\mathrm{s}$).

3.2. *Results*

Comparing the solutions obtained with different realizations of the model dynamics is difficult because of the non-linear feedback of the ice dynamics and thermodynamics. Already after a few months the solutions have diverged so far from each other

Table 1
Overview over model simulations in Section 3.2.

experiment name	description
B-LSR-ns	the original LSOR solver of Zhang and Hibler (1997) on an Arakawa B-grid, implying no-slip lateral boundary conditions ($\mathbf{u} = 0$ exactly), advection of ice variables with a 2nd-order central difference scheme plus explicit diffusion for stability
C-LSR-ns	the LSOR solver discretized on a C-grid with no-slip lateral boundary conditions (implemented via ghost-points)
C-LSR-fs	the LSOR solver on a C-grid with free-slip lateral boundary conditions
C-EVP-ns	the EVP solver of Hunke (2001) on a C-grid with no-slip lateral boundary conditions and $\Delta t_{\text{evp}} = 150\,\text{s}$
C-EVP-ns10	the EVP solver of Hunke (2001) on a C-grid with no-slip lateral boundary conditions and $\Delta t_{\text{evp}} = 10\,\text{s}$
C-LSR-ns HB87	C-LSR-ns with ocean-ice stress coupling according to Hibler and Bryan (1987)
C-LSR-ns TEM	C-LSR-ns with a truncated ellispe method (TEM) rheology (Hibler and Schulson, 1997)
C-LSR-ns WTD	C-LSR-ns with 3-layer thermodynamics following Winton (2000)
C-LSR-ns DST3FL	C-LSR-ns with a third-order flux limited direct-space-time advection scheme for thermodynamic variables (Hundsdorfer and Trompert, 1994)

that comparing velocities only makes sense within the first 3 months of the integration while the ice distribution is still close to the initial conditions. At the end of the integration, the differences between the model solutions can be interpreted as cumulated model uncertainties.

3.2.1. *Ice velocities in JFM 1992*

Figure 3 shows ice velocities averaged over Janunary, February, and March (JFM) of 1992 for the C-LSR-ns solution; also shown are the differences between this reference solution and various sensitivity experiments. The velocity field of the C-LSR-ns solution (Figure 3a) roughly resembles the drift velocities of some of the AOMIP (Arctic Ocean Model Intercomparison Project) models in a cyclonic circulation regime (CCR) (Martin and Gerdes, 2007, their Figure 6) with a Beaufort Gyre and a transpolar drift shifted eastwards towards Alaska.

The difference beween runs C-LSR-ns and B-LSR-ns (Figure 3b) is most pronounced along the coastlines, where the discretization differs most between B and C-grids: On a B-grid the tangential velocity lies on the boundary (and is thus zero through the no-slip boundary conditions), whereas on the C-grid it is half a cell width away from the boundary, thus allowing more flow. The B-LSR-ns solution has less ice drift through the Fram Strait and along Greenland's east coast; also, the flow through Baffin Bay and Davis Strait into the Labrador Sea is reduced with respect the C-LSR-ns solution. *[Do we expect this? Say something about that]* Compared to the differences between B and C-grid solutions, the C-LSR-fs ice drift field differs much less from the C-LSR-ns solution (Figure 3c). As expected the differences are largest along coastlines: because of the free-slip boundary conditions, flow is faster in the C-LSR-fs solution, for example, along the east coast of Greenland, the north coast of Alaska, and the east Coast of Baffin Island.

The C-EVP-ns solution with $\Delta t_{\text{evp}} = 150\,\text{s}$ is very different from the C-LSR-ns solution (Figure 3d). The EVP-approximation of the VP-dynamics allows for increased drift by up to 8 cm/s in the Beaufort Gyre and the transarctic drift. In general, drift velocities are strongly biased towards higher values in the EVP solutions.

Compared to the other parameters, the ice rheology TEM (Figure 3e) has a very small effect on the solution. In general the ice drift tends to be increased, because there is no tensile stress and ice can be "pulled appart" at no cost. Consequently, the largest effect on drift velocity can be observed near the ice edge in the Labrador Sea. In contrast, the drift is stronger almost everywhere in the computational domain in the run with the ice-ocean stress formulation of Hibler and Bryan (1987) (Figure 3f). The increase is mostly aligned with the general direction of the flow, implying that the different stress formulation reduces the deceleration of drift by the ocean.

The 3-layer thermodynamics following Winton (2000) requires additional information on initial conditions for enthalphy. These different initial conditions make a comparison of the first months difficult to interpret. The drift in the Beaufort Gyre is slightly reduced relative to the reference run C-LSR-ns, but the drift through the Fram Strait is increased. The drift velocities near the ice edge are very different, because the ice extend is already larger in C-LSR-ns WTD; inward from the ice egde,

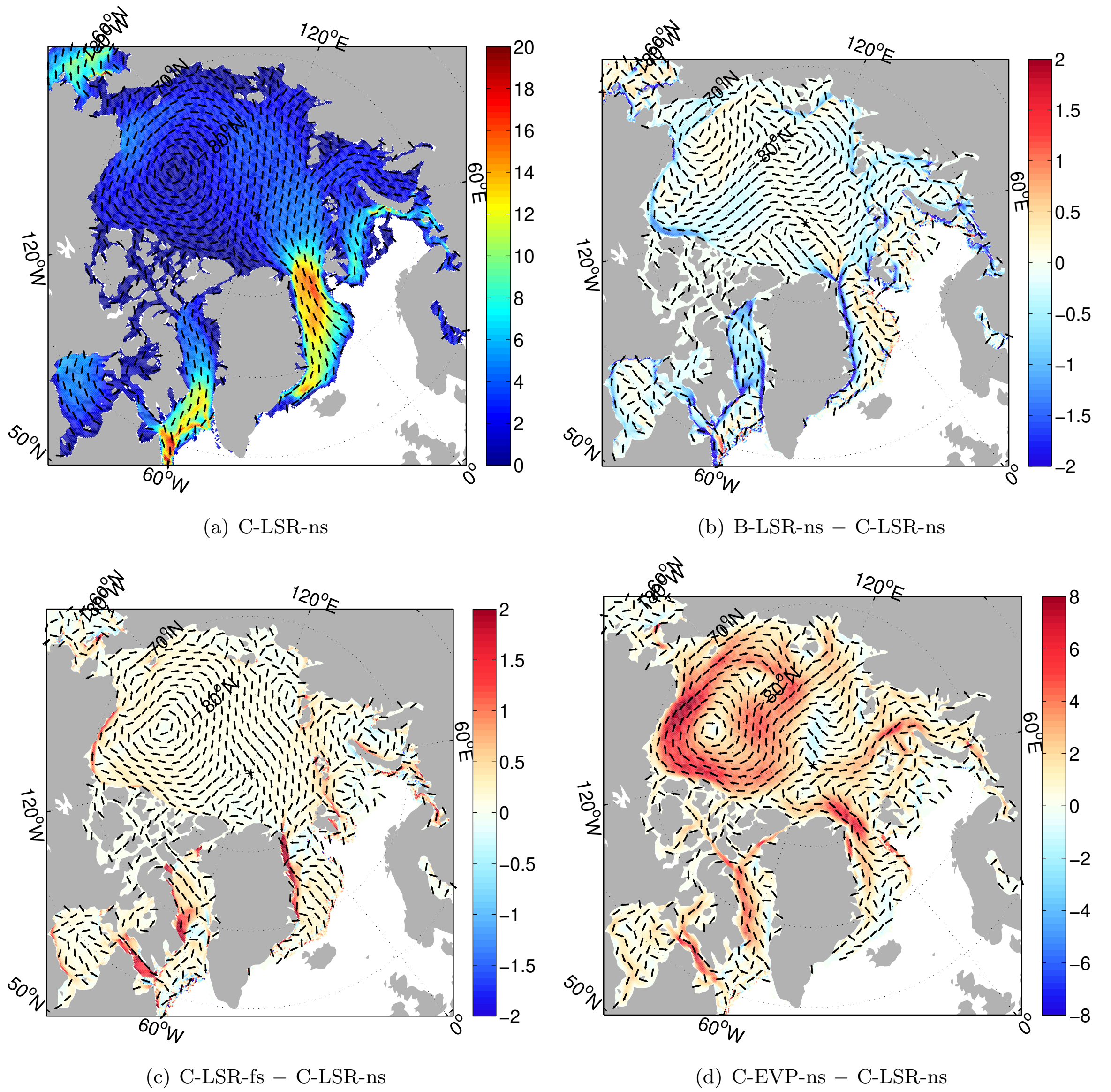

(a) C-LSR-ns

(b) B-LSR-ns − C-LSR-ns

(c) C-LSR-fs − C-LSR-ns

(d) C-EVP-ns − C-LSR-ns

Fig. 3. (a) Ice drift velocity of the C-LSR-ns solution averaged over the first 3 months of integration [cm/s]; (b)-(h) difference between solutions with B-grid, free lateral slip, EVP-solver, truncated ellipse method (TEM), different ice-ocean stress formulation (HB87), different thermodynamics (WTD), different advection for thermodynamic variables (DST3FL) and the C-LSR-ns reference solution [cm/s]; color indicates speed (or differences of speed), vectors indicate direction only.

this run has smaller drift velocities, because the ice motion is more contrained by a larger ice extent than in C-LSR-ns, where the ice at the same geographical position is nearly in free drift.

A more sophisticated advection scheme (C-LSR-ns DST3FL, Figure 3h) has some effect along the ice edge, where the gradients of thickness and concentration are largest. Everywhere else the effect is very small and can mostly be attributed to smaller numerical diffusion (and to the absense of explicit diffusion that is requird for numerical stability in a simple second order central differences scheme).

3.2.2. *Ice volume during JFM 2000*

Figure 4a shows the effective thickness (volume per unit area) of the C-LSR-ns solution, averaged over January, February, March of year 2000. By this time of the integration, the differences in the ice drift velocities have led to the evolution of very different

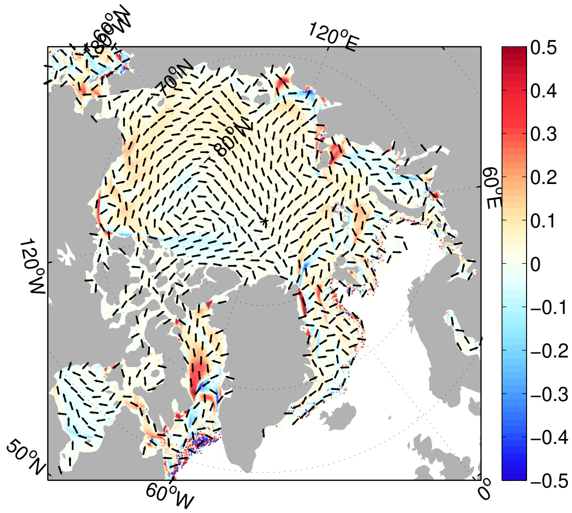

(e) C-LSR-ns TEM − C-LSR-ns

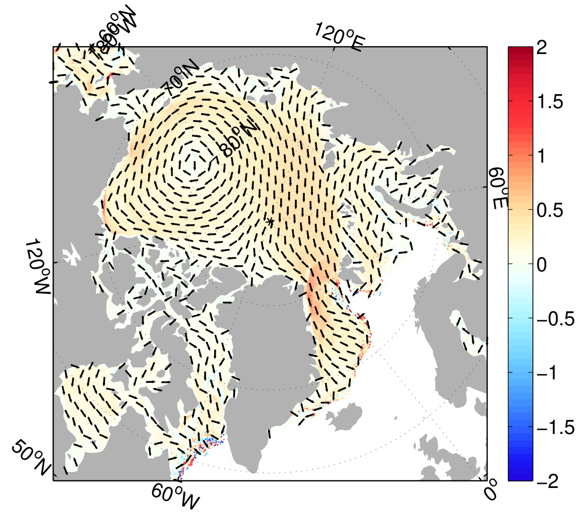

(f) C-LSR-ns HB87 − C-LSR-ns

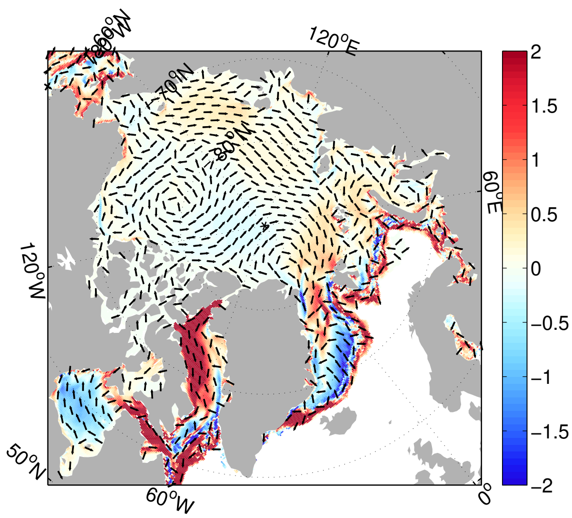

(g) C-LSR-ns WTD − C-LSR-ns

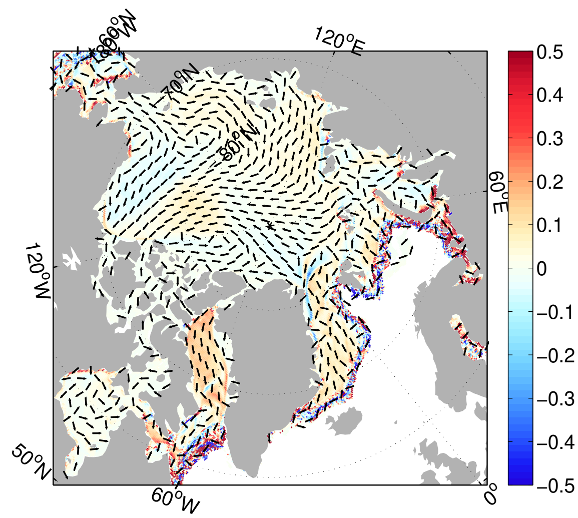

(h) C-LSR-ns DST3FL − C-LSR-ns

Fig. 3. continued

ice thickness distributions, which are shown in Figure 4b–h, and concentrations (not shown). The generally weaker ice drift velocities in the B-LSR-ns solution, when compared to the C-LSR-ns solution, in particular through the narrow passages in the Canadian Arctic Archipelago, lead to a larger build-up of ice north of Greenland and the Archipelago by 2 m effective thickness and more in the B-grid solution (Figure 4b). But the ice volume in not larger everywhere: further west, there are patches of smaller ice volume in the B-grid solution, most likely because the Beaufort Gyre is weaker and hence not as effective in transporting ice westwards. There are also dipoles of ice volume differences with more ice on the upstream side of island groups and less ice in their lee, such as Franz-Josef-Land and Severnaya Semlya*/or Nordland?*, because ice tends to flow along coasts less easily in the B-LSR-ns solution.

Imposing a free-slip boundary condition in C-LSR-fs leads to much smaller differences to C-LSR-ns in the central Arctic than the transition from the B-grid to the C-grid (Figure 4c), except in the Canadian Arctic Archipelago. There it reduces the effective ice thickness by 2 m and more where the ice is thick and the straits are narrow. Dipoles of ice thickness differences can also be observed around

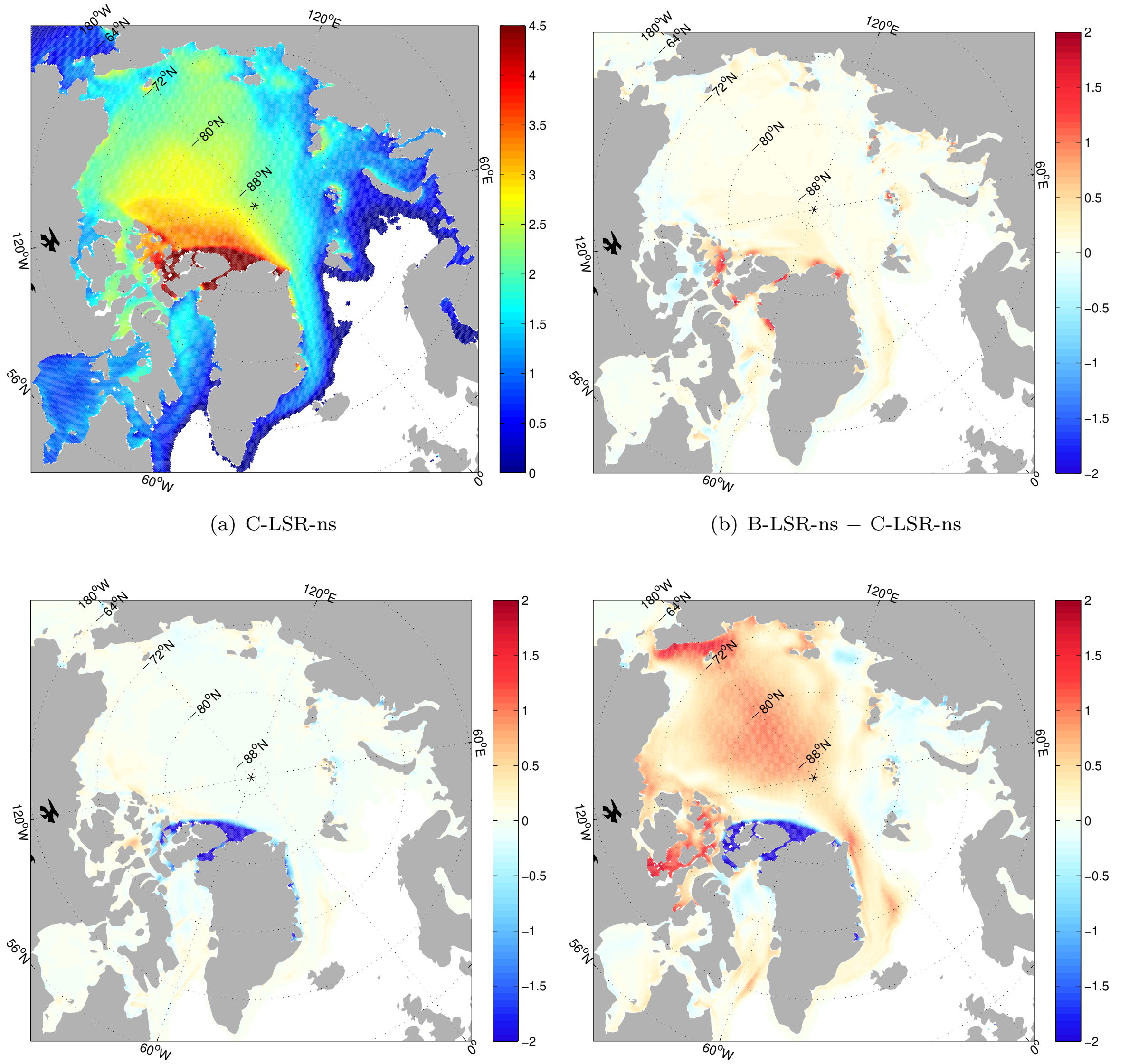

(a) C-LSR-ns

(b) B-LSR-ns − C-LSR-ns

(c) C-LSR-fs − C-LSR-ns

(d) C-EVP-ns − C-LSR-ns

Fig. 4. (a) Effective thickness (volume per unit area) of the C-LSR-ns solution, averaged over the months Janurary through March 2000 [m]; (b)-(h) difference between solutions with B-grid, free lateral slip, EVP-solver, truncated ellipse method (TEM), different ice-ocean stress formulation (HB87), different thermodynamics (WTD), different advection for thermodynamic variables (DST3FL) and the C-LSR-ns reference solution [m].

islands, because the free-slip solution allows more flow around islands than the no-slip solution. Everywhere else the ice volume is affected only slightly by the different boundary condition. The C-EVP-ns solution has much thicker ice in the central Arctic Ocean than the C-LSR-ns solution (Figure 4d, note the color scale). Within the Canadian Arctic Archipelago, more drift leads to faster ice export and reduced effective ice thickness. With a shorter time step of $\Delta t_{\mathrm{evp}} = 10\,\mathrm{s}$ the EVP solution converges to the LSOR solution (not shown). Only in the narrow straits in the Archipelago the ice thickness is not affected by the shorter time step and the ice is still thinner by 2 m and more, as in the EVP solution with $\Delta t_{\mathrm{evp}} = 150\,\mathrm{s}$.

In year 2000, there is more ice everywhere in the domain in C-LSR-ns WTD (Figure 4g, note the color scale). This difference, which is even more pro-

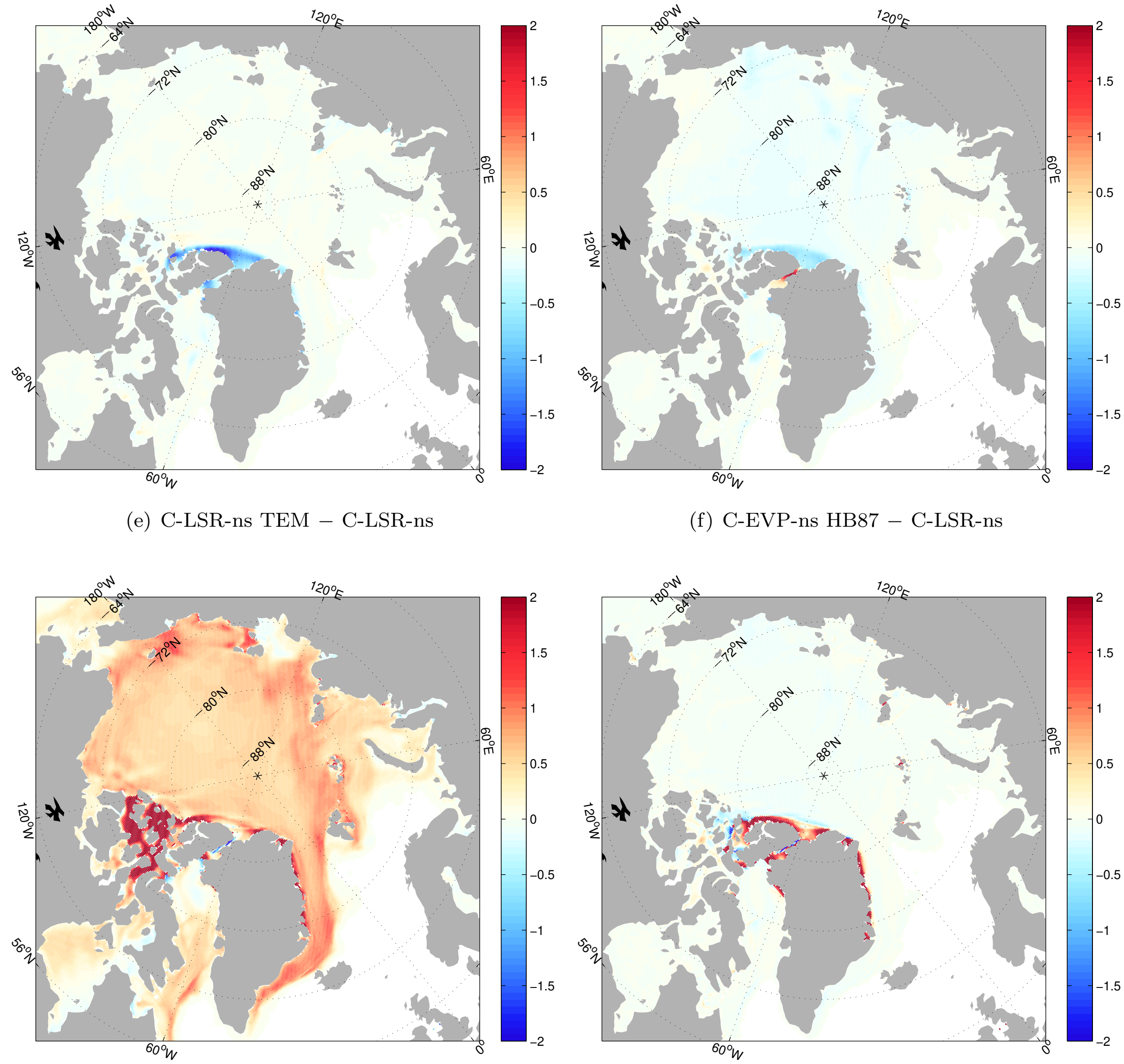

(e) C-LSR-ns TEM − C-LSR-ns

(f) C-EVP-ns HB87 − C-LSR-ns

(g) C-LSR-ns WTD − C-LSR-ns

(h) C-EVP-ns DST3FL − C-LSR-ns

Fig. 4. continued

nounced in summer (not shown), can be attributed to direct effects of the different thermodynamics in this run. The remaining runs have the largest differences in effective ice thickness long the north coasts of Greenland and Ellesmere Island. Although the effects of TEM and Hibler and Bryan (1987)'s ice-ocean stress formulation are so different on the initial ice velocities, both runs have similarly reduced ice thicknesses in this area. The 3rd-order advection scheme has an opposite effect of similar magnitude, pointing towards more implicit lateral stress with this numerical scheme.

The observed difference of order 2 m and less are smaller than the differences that were observed between different hindcast models and climate models in Gerdes and Köberle (2007). There the range of sea ice volume of different sea ice-ocean models (which shared very similar forcing fields) was on the order of $10,000\text{km}^3$; this range was even larger for coupled climate models. Here, the range (and the averaging period) is smaller than $4,000\text{km}^3$ except for the run C-LSR-ns WTD where the more complicated thermodynamics leads to generally thicker ice (Figure 4 and Table 2).

Table 2
Arctic ice volume averaged over Jan–Mar 2000, in km^3. Mean ice transport and standard deviation for the period Jan 1992 – Dec 1999 through the Fram Strait (FS), the total northern inflow into the Canadian Arctic Archipelago (NI), and the export through Lancaster Sound (LS), in $\mathrm{km}^3\,\mathrm{y}^{-1}$.

model run	ice volume	ice transport [flux± std., $\mathrm{km}^3\,\mathrm{y}^{-1}$]		
	[km^3]	FS	NI	LS
B-LSR-ns	23,824	2126±1278	34±122	43± 76
C-LSR-ns	24,769	2196±1253	70±224	77± 110
C-LSR-fs	23,286	2236±1289	80±276	91± 85
C-EVP-ns	27,056	3050±1652	352±735	256± 151
C-EVP-ns10	22,633	2174±1260	186±496	133± 128
C-LSR-ns HB87	23,060	2256±1327	64±230	77± 114
C-LSR-ns TEM	23,529	2222±1258	60±242	87± 112
C-LSR-ns WTD	31,634	2761±1563	23±140	94± 63
C-LSR-ns DST3FL	24,023	2191±1261	88±251	84± 129

3.2.3. *Ice transports*

The difference in ice volume and ice drift velocities between the different experiments has consequences for the ice transport out of the Arctic. Although by far the most exported ice drifts through the Fram Strait (approximately $2300\pm610\,\mathrm{km}^3\,\mathrm{y}^{-1}$), a considerable amount (order $160\,\mathrm{km}^3\,\mathrm{y}^{-1}$) ice is exported through the Canadian Arctic Archipelago (Serreze et al., 2006, and references therein). Note, that ice transport estimates are associated with large uncertainties; also note that tuning an Arctic sea ice-ocean model to reproduce observations is not our goal, but we use the published numbers as an orientation.

Figure 5 shows an excerpt of a time series of daily averaged ice transports, smoothed with a monthly running mean, through various straits in the Canadian Arctic Archipelago and the Fram Strait for the different model solutions; Table 2 summarizes the time series. The export through Fram Strait agrees with the observations in all model solutions (annual averages range from 2110 to $2300\,\mathrm{km}^3\,\mathrm{y}^{-1}$, except for C-LSR-ns WTD with $2760\,\mathrm{km}^3\,\mathrm{y}^{-1}$ and the EVP solution with the long time step of 150 s with nearly $3000\,\mathrm{km}^3\,\mathrm{y}^{-1}$), while the export through the Candian Arctic Archipelago is smaller than generally thought. For example, the ice transport through Lancaster Sound is lower (annual averages are 43 to $256\,\mathrm{km}^3\,\mathrm{y}^{-1}$) than in Dey (1981) who estimates an inflow into Baffin Bay of 370 to $537\,\mathrm{km}^3\,\mathrm{y}^{-1}$, but a flow of only 102 to $137\,\mathrm{km}^3\,\mathrm{y}^{-1}$ further upstream in Barrow Strait in the 1970ies from satellite images. Generally, the EVP solutions have the highest maximum (export out of the Artic) and lowest minimum (import into the Artic) fluxes as the drift velocities are largest in these solutions. In the extreme of the Nares Strait, which is only a few grid points wide in our configuration, both B- and C-grid LSOR solvers lead to practically no ice transport, while the C-EVP solutions allow up to $600\,\mathrm{km}^3\,\mathrm{y}^{-1}$ in summer (not shown); Tang et al. (2004) report 300 to $350\,\mathrm{km}^3\,\mathrm{y}^{-1}$. As as consequence, the import into the Candian Arctic Archipelago is larger in all EVP solutions than in the LSOR solutions. The B-LSR-ns solution is even smaller by another factor of two than the C-LSR solutions (an exception is the WTD solution, where larger ice thickness tends to block the transport).

3.2.4. *Discussion*

In summary, we find that different dynamical solvers can yield very different solutions. In constrast to that, the differences between free-slip and no-slip solutions *with the same solver* are considerably smaller (the difference for the EVP solver is not shown, but similar to that for the LSOR solver). Albeit smaller, the differences between free and no-slip solutions in ice drift can lead to equally large differences in ice volume, especially in the Canadian Arctic Archipelago over the integration time. At first, this observation seems counterintuitive, as we expect that the solution *technique* should not affect the *solution* to a higher degree than actually modifying the equations. A more detailed study on these differences is beyond the scope of this paper, but at this point we may speculate, that the large difference between B-grid, C-grid, LSOR, and EVP solutions

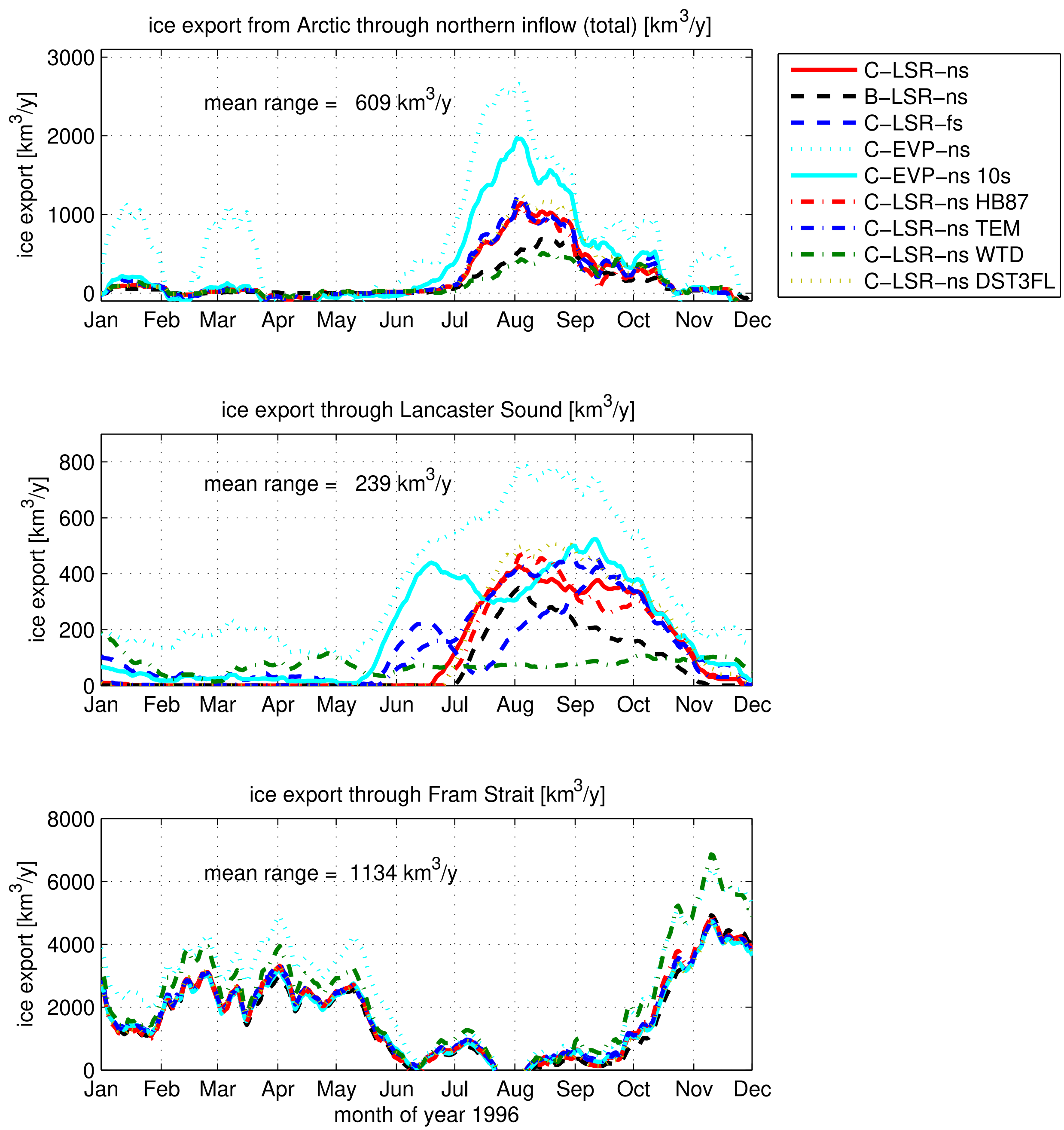

Fig. 5. Transport through Canadian Arctic Archipelago for different solver flavors. The sections labeled in Figure 1; positive values are flux out of the Arctic; legend abbreviations are explained in Table 1. The mean range of the different model solutions is taken over the period Jan 1992 to Dec 1999.

stem from incomplete convergence of the solvers due to linearization and due to different methods of linearization (Hunke, 2001, and Bruno Tremblay, personal communication): if the convergence of the non-linear momentum equations is not complete for all linearized solvers, then one can imagine that each solver stops at a different point in velocity-space thus leading to different solutions for the ice drift velocities. If this were true, this tantalizing circumstance would have a dramatic impact on sea-ice modeling in general, and we would need to improve the solution techniques for dynamic sea ice models, most likely at a very high compuational cost (Bruno Tremblay, personal communication).

Further, we observe that the EVP solutions tend to produce effectively "weaker" ice that yields more easily to stress. This was also observed by Hunke and Zhang (1999) in a fast response to changing winds, their Figures 10–12, where the EVP model adjusts quickly to a cyclonic wind pattern, while the LSOR solution lags in time. This property of the EVP solutions allows larger ice transports through narrow straits, where the implicit solver LSOR forms rigid ice. The underlying reasons for this striking difference need further exploration.

4. Conclusions and Recommendations

Modeling sea-ice is a serious challenge. Uncertainties in discretization details, boundary conditions, model physics and parameterizations lead to considerable differences in model results. We do not attempt to decide which of the different sea-ice model realizations is "the best" because *[ML: can we say that?] there are simply not enough observations available (?) and* the criteria by which this decision should be made is unclear. However, we can give recommendations for the usage of the MITsim (and possibly other similar sea-ice models) based on the comparison of different features, which this sea-ice model combines in one code. Specifically:

- We recommend to use the LSOR or another implicit solver, because EVP tends to have too weak ice leading to much larger ice drift velocities and ice export solutions than found in all other solutions. Further, in spite of its simpler algorithm, which yields itself to easily to MPI parallelization, our EVP code is much slower for the recommended time step choices ($\frac{1}{120}$ of the model time step): The integrations times for one model year of the Arctic model presented in this paper are *[Dimitris: ??? hours for an LSOR solution, and ??? hours for an EVP solution with 120 sub-cycling time steps within one time step (20 min), and ??? hours for an EVP solutions 120 sub-cycling time steps within one forcing cycle (6 hours) XX CPUs on a SGI Altix computer.* Linearization as discussed in Hunke (2001) does not appear to be an issue for the short time steps used in this study ($\Delta t = 20\,\text{min}$); the LSOR-solver converges quickly (only a few iterations) at each time step, because the 6-hourly forcing changes only slowly within the 20 min time step.
- After the choice of the dynamical solver, the specifics of the thermodynamics appear to have the second largest effect. As expected the three-layer thermodynamics following Winton (2000) lead to larger ice volumes (and also greater ice extend in summer, not shown). Observations of ice thickness are rare and parameter tuning is not complete for any model, so that it is too early to claim that one or the other solutions is superior. The Winton (2000) thermodynamics clearly contain more realistic physical notions than the zero-layer model.
- A flux limited scheme without explicit diffusion for advecting thermodynamic variables, especially near the ice-edge makes the most sense, although the impact on the solution is comparatively small except near coasts.
- No slip boundary conditions make more sense intuitivley, but as long as the complicated boundary layer along the coast cannot be resolved, free slip boundaries conditions cannot be discarded.
- Changing the ice rheology to the trucated ellipse method (TEM) has little effect on the solution, other rheologies that differ more from the elliptic yield curve may have bigger effects.
- Hibler and Bryan (1987)'s stress formulation appears more natural, but the effect on the ice solution is small. We did not explore its impact on the ocean model solution. For the ocean, we expect larger effects, especially for ocean models with high vertical resolution, because of the inconsistency of advecting thermodynamic properties of the ocean with a velocity that is the average over ice drift and ocean currents.

The above recommendations may or may not hold for other sea ice models. However, the MITsim makes the direct comparisons within the same code possible. This capability supports the systematic parameter studies that are described in Part 2. The second part is devoted to the important feature of the code that its structure allows the automatic generation of efficient adjoint (derivative) code within the framework of the MITgcm. The adjoint model greatly facilitates exploring the parameter space of the model with the help of linearized sensitivies. However, the effects of switching on different features cannot be explored by an adjoint model. Comparisons of different code configurations as presented here are also necessary for evaluating sensitivites with the help of adjoint and will be presented in Part 2.

Acknowledgements

We thank Jinlun Zhang for providing the original B-grid code and many helpful discussions. ML thanks Elizabeth Hunke for multiple explanations.

This work is a contribution to Estimating the Circulation and Climate of the Ocean, Phase II (ECCO2). The ECCO2 project (http://ecco2.org/) is sponsored by the NASA Modeling Analysis and Prediction (MAP) program. D. Menemenlis carried out this work at the Jet Propulsion Laboratory, California Institute of Technology under contract with the National Aeronautics and Space Administration.

References

Adcroft, A., Campin, J.-M., Hill, C. N., Marshall, J. C., 2004. Implementation of an atmosphere-ocean general circulation model on the expanded spherical cube. Mon. Weather Rev. 132 (12), 2845–2863.

Adcroft, A., Hill, C., Marshall, J., 1997. Representation of topography by shaved cells in a height coordinate ocean model. Mon. Weather Rev. 125 (9), 2293–2315.

Adcroft, A., Marshall, D., 1998. How slippery are piecewise-constant coastlines in numerical ocean models? Tellus 50A, 95–108.

Bryan, K., Lewis, L. J., 1979. A water mass model of the world ocean. J. Geophys. Res. 84, 2503–2517.

Campin, J.-M., Marshall, J., Ferreira, D., 2008. Sea-ice ocean coupling using a rescaled vertical coordinate z^*. Ocean Modelling 24 (1–2), 1–14.

Cavalieri, D. J., Parkinson, C., 2008. Antarctic sea ice variability and trends, 1979–2006. J. Geophys. Res. 113, C07004.

Daru, V., Tenaud, C., 2004. High order one-step monotonicity-preserving schemes for unsteady compressible flow calculations. J. Comput. Phys. 193 (2), 563–594.

Dey, B., 1981. Monitoring winter sea ice dynamics in the Canadian Arctic with NOAA-TIR images. J. Geophys. Res. 86 (C4), 3223–3235.

Dutkiewicz, S., Follows, M., Heimbach, P., Marshall, J., 2006. Controls on ocean productivity and air-sea carbon flux: An adjoint model sensitivity study. Geophys. Res. Lett. 33, L02603.

Fox-Kemper, B., Menemenlis, D., 2008. Can large eddy simulation techniques improve mesoscale rich ocean models? In: Hecht, M., Hasumi, H. (Eds.), Ocean Modeling in an Eddying Regime. AGU, Washington, D.C., pp. 319–338.

Fukumori, I., 2002. A partitioned Kalman filter and smoother. Mon. Weather Rev. 130, 1370–1383.

Geiger, C. A., Hibler, III, W. D., Ackley, S. F., 1998. Large-scale sea ice drift and deformation: Comparison between models and observations in the western Weddell Sea during 1992. J. Geophys. Res. 103 (C10), 21893–21913.

Gerdes, R., Köberle, C., 2007. Comparison of Arctic sea ice thickness variability in IPCC Climate of the 20th Century experiments and in ocean-sea ice hindcasts. J. Geophys. Res. 112 (CO4S13).

Griewank, A., 2000. Evaluating Derivatives. Principles and Techniques of Algorithmic Differentiation. Vol. 19 of Frontiers in Applied Mathematics. SIAM, Philadelphia.

Harder, M., Fischer, H., 1999. Sea ice dynamics in the Weddell Sea simulated with an optimzed model. J. Geophys. Res. 104 (C5), 11,151–11,162.

Heimbach, P., Wunsch, C., 2007. Estimating the Circulation and Climate of the Ocean – The ECCO Consortia. U.S. CLIVAR Variations V5N3, .

Hibler, III, W. D., 1979. A dynamic thermodynamic sea ice model. J. Phys. Oceanogr. 9 (4), 815–846.

Hibler, III, W. D., 1980. Modeling a variable thickness sea ice cover. Mon. Weather Rev. 108 (2), 1943–1973.

Hibler, III, W. D., 1984. The role of sea ice dynamics in modeling co_2 increases. In: Hansen, J. E., Takahashi, T. (Eds.), Climate processes and climate sensitivity. Vol. 29 of Geophysical Monograph. AGU, Washington, D.C., pp. 238–253.

Hibler, III, W. D., Bryan, K., 1987. A diagnostic ice-ocean model. J. Phys. Oceanogr. 17 (7), 987–1015.

Hibler, III, W. D., Ip, C. F., 1995. The effect of sea ice rheology on Arcitc buoy drift. In: Dempsey, J. P., Rajapakse, Y. D. S. (Eds.), Ice Mechanics. Vol. 204 of AMD. Am. Soc. of Mech. Eng., New York, pp. 255–264.

Hibler, III, W. D., Schulson, E. M., 1997. On modeling sea-ice fracture and flow in numerical investigations of climate. Ann. Glaciol. 25, 26–32.

Holloway, G., Dupont, F., Golubeva, E., Häkkinen, S., Hunke, E., Jin, M., Karcher, M., Kauker, F., Maltrud, M., Morales Maqueda, M. A., Maslowskski, W., Platov, G., Stark, D., Steele, M., Suzuki, T., Wang, J., Zhang, J., 2007. Water properties and circulation in Arctic Ocean models. J. Geophys. Res. 112 (C04S03).

Huffman, G. J., Adler, R. F., Morrissey, M. M., Curtis, S., Joyce, R., McGavock, B., Susskind, J., 2001. Global precipitation at one-degree daily resolution from multi-satellite observations. J. Hydrometeor. 2, 36–50.

Hundsdorfer, W., Trompert, R. A., 1994. Method of lines and direct discretization: a comparison for linear advection. Applied Numerical Mathematics 13 (6), 469–490.

Hunke, E. C., 2001. Viscous-plastic sea ice dynamics with the EVP model: Linearization issues. J. Comp. Phys. 170, 18–38.

Hunke, E. C., Dukowicz, J. K., 1997. An elastic-viscous-plastic model for sea ice dynamics. J. Phys. Oceanogr. 27, 1849–1867.

Hunke, E. C., Zhang, Y., 1999. A comparison of sea ice dynamics models at high resolution. Mon. Weather Rev. 127, 396–408.

Ip, C. F., Hibler, III, W. D., Flato, G. M., 1991. On the effect of rheology on seasonal sea-ice simulations. Ann. Glaciol. 15, 17–25.

Jackett, D. R., McDougall, T. J., 1995. Minimal adjustment of hydrographic profiles to achieve static stability. J. Atmos. Oceanic Technol. 12, 381–389.

Kreyscher, M., Harder, M., Lemke, P., Flato, G. M., 2000. Results of the Sea Ice Model Intercomparison Project: Evaluation of sea ice reology schemes for use in climate simulations. J. Geophys. Res. 105 (C5), 11,299–11,320.

Large, W. G., McWilliams, J. C., Doney, S., 1994. Oceanic vertical mixing: A review and a model with a nonlocal boundary layer parameterization. Rev. Geophysics 32, 363–403.

Large, W. G., Nurser, A. J. G., 2001. Ocean surface water mass transformation. In: Siedler, G., Church, J., Gould, J. (Eds.), Ocean Circulation and Climate. Academic, San Diego, Calif., pp. 317–336.

Large, W. G., Pond, S., 1981. Open ocean momentum flux measurements in moderate to strong winds. J. Phys. Oceanogr. 11, 324–336.

Large, W. G., Pond, S., 1982. Sensible and latent heat flux measurements over the ocean. J. Phys. Oceanogr. 12, 464–482.

Leith, C. E., 1996. Stochastic models of chaotic systems. Physica D 98, 481–491.

Lemieux, J.-F., Tremblay, B., Thomas, S., Sedláček, J., Mysak, L. A., 2008. Using the preconditioned Generalized Minimum RESidual (GMRES) method to solve the sea-ice momentum equation. J. Geophys. Res. in press.

Lemke, P., Ren, J., Alley, R. B., Allison, I., Carrasco, J., Flato, G., Fujii, Y., Kaser, G., Mote, P., Thomas, R. H., Zhang, T., 2007. Observations: Changes in snow, ice and frozen ground. In: Solomon, S., Qin, D., Manning, M., Chen, Z., Marquis, M., Averyt, K. B., Tignor, M., Miller, H. L. (Eds.), Climate Change 2007: The Physical Science Basis. Contribution of Working Group I to the Fourth Assessment Report of the Intergovernmental Panel on Climate Change. Cambridge University Press, Cambridge, United Kingdom and New York, NY, USA, pp. 338–383.

Leppäranta, M., 1983. A growth model for black ice, snow ican and snow thickness in subarctic basins. Nordic Hydrology 14, 59–70.

Lohmann, G., Gerdes, R., 1998. Sea ice effects on the sensitivity of the thermohaline circulation in simplified atmosphere-ocean-sea ice models. J. Climate 11, 2789–2803.

Losch, M., Heimbach, P., 2007. Adjoint sensitivity of an ocean general circulation model to bottom topography. J. Phys. Oceanogr. 37(2), 377–393.

Manabe, S., Bryan, K., Spelman, M. J., 1979. A global ocean-atmosphere climate model with seasonal variation for future studies of climate sensitivity. Dyn. Atmos. Oceans 3 (393–426).

Marotzke, J., Giering, R., Zang, K. Q., Stammer, D., Hill, C., Lee, T., 1999. Construction of the adjoint MIT ocean general circulation model and application to Atlantic heat transport sensitivity. J. Geophys. Res. 104 (C12), 29529–29547.

Marshall, J., Adcroft, A., Hill, C., Perelman, L., Heisey, C., 1997a. A finite-volume, incompressible Navier Stokes model for studies of the ocean on parallel computers. J. Geophys. Res. 102 (C3), 5753–5766.

Marshall, J., Hill, C., Perelman, L., Adcroft, A., 1997b. Hydrostatic, quasi-hydrostatic, and nonhydrostatic ocean modeling. J. Geophys. Res. 102 (C3), 5733–5752.

Martin, T., Gerdes, R., 2007. Sea ice drift variability in Arctic Ocean Model Intercomparison Project models and observations. J. Geophys.

Res. 112 (C04S10).
McPhee, M. G., 1992. Turbulent heat flux in the upper ocean under sea ice. J. Geophys. Res. 97 (C4), 5365–5379.
Mellor, G. L., McPhee, M. G., Steele, M., 1986. Ice-seawater turbulent boundary layer interaction with melting or freezing. J. Phys. Oceanogr. 16 (11), 1829–1846.
Menemenlis, D., Fukumori, I., Lee, T., 2005a. Using Green's functions to calibrate an ocean general circulation model. Mon. Weather Rev. 133, 1224–1240.
Menemenlis, D., Hill, C., Adcroft, A., Campin, J.-M., Cheng, B., Ciotti, B., Fukumori, I., Koehl, A., Heimbach, P., Henze, C., Lee, T., Stammer, D., Taft, J., Zhang, J., 2005b. NASA supercomputer improves prospects for ocean climate research. Eos Trans. AGU 86 (9), 89, 95–96.
MITgcm Group, 2002. MITgcm Release 1 Manual. Online documentation, MIT/EAPS, Cambridge, MA 02139, USA, `http://mitgcm.org/sealion/online_documents/manual.html`.
Notz, D., McPhee, M. G., Worster, M. G., Maykut, G. A., Schlünzen, K. H., , Eicken, H., 2003. Impact of underwater-ice evolution on Arctic summer sea ice. J. Geophys. Res. 108 (C7), 3223.
Parkinson, C. L., Cavalieri, D., 2008. Arctic sea ice variability and trends, 1979–2006. J. Geophys. Res. 113, C07003.
Parkinson, C. L., Washington, W. M., Jan. 1979. A Large-Scale Numerical Model of Sea Ice. J. Geophys. Res. 84 (C1), 311–337.
Paulson, C. A., Simpson, J. J., 1977. Irradiance measurements in the upper ocean. J. Phys. Oceanogr. 7, 952–956.
Roe, P., 1985. Some contributions to the modelling of discontinuous flows. In: Engquist, B., Osher, S., Somerville, R. (Eds.), Large-Scale Computations in Fluid Mechanics. Vol. 22 of Lectures in Applied Mathematics. American Mathematical Society, pp. 163–193.
Semtner, Jr., A. J., 1976. A model for the thermodynamic growth of sea ice in numerical investigations of climate. J. Phys. Oceanogr. 6, 379–389.
Semtner, Jr., A. J., 1984. On modelling the seasonal thermodynamic cycle of sea ice in studies of climatic change. Clim. Change 6 (1), 27–37.
Serreze, M. C., Barrett, A. P., Slater, A. G., Woodgate, R. A., Aagaard, K., Lammers, R. B., Steele, M., Moritz, R., Meredith, M., Lee, C. M., 2006. The large-scale freshwater cycle of the Arctic. J. Geophys. Res. 111 (C11010).
Smith, W. H. F., Sandwell, D. T., 1997. Global sea floor topography from satellite altimetry and ship depth soundings. Science 277, 1956–1962.
Steele, M., Morley, R., Ermold, W., 2001. Phc: A global ocean hydrography with a high quality arctic ocean. J. Clim. 14, 2079–2087.
Tang, C. C. L., Ross, C. K., Yao, T., Petrie, B., DeTracey, B. M., Dunlap, E., December 2004. The circulation, water masses and sea-ice of Baffin Bay. Prog. Oceanogr. 63 (4), 183–228.
Timmermann, R., Beckmann, A., Hellmer, H. H., 2002. Simulation of ice-ocean dynamics in the Weddell Sea. Part I: Model configuration and validation. J. Geophys. Res. 107 (C3), 3024.
Tremblay, L.-B., Mysak, L. A., 1997. Modeling sea ice as a granular material, including the dilatancy effect. J. Phys. Oceanogr. 27, 2342–2360.
Uppala, S. M., Kållberg, P. W., Simmons, A. J., Andrae, U., da Costa Bechtold, V., Fiorino, M., Gibson, J. K., Haseler, J., Hernandez, A., Kelly, G. A., Li, X., Onogi, K., Saarinen, S., Sokka, N., Allan, R., Andersson, E., Arpe, K., Balmaseda, M., Beljaars, A., van de Berg, L., Bidlot, J., Bormann, N., Caires, S., Chevallier, F., Dethof, A., Dragosavac, M., Fisher, M., Fuentes, M., Hagemann, S., Hólm, E., Hoskins, B., Isaksen, L., Janssen, P., Jenne, R., McNally, A., Mahfouf, J.-F., Morcrette, J.-J., Rayner, N., Saunders, R., Simon, P., Sterl, A., Trenberth, K., Untch, A., Vasiljevic, D., Viterbo, P., Woollen, J., 2005. The era-40 re-analysis. Q. J. R. Meteorol. Soc. 131, 2961–3012.
Winton, M., 2000. A reformulated three-layer sea ice model. J. Atmos. Oceanic Technol. 17 (4), 525–531.
Wunsch, C., Heimbach, P., 2007. Practical global oceanic state estimation. Physica D 230(1-2), 197–208.
Zhang, J., Hibler, III, W. D., 1997. On an efficient numerical method for modeling sea ice dynamics. J. Geophys. Res. 102 (C4), 8691–8702.
Zhang, J., Hibler, III, W. D., Steele, M., Rothrock, D. A., 1998. Artic ice-ocean modeling with and without climate restoring. J. Phys. Oceanogr. 28 (2), 191–217.
Zhang, J., Rothrock, D. A., 2003. Modeling global sea ice with a thickness and enthalpy distribution model in generalized curvilinear coordinates. Mon. Weather Rev. 131 (5), 845–861.